Preprint Title	Room-temperature high-performance ammonia gas sensor based on hydroxyapatite film
Authors	Mingxu Sun, Ziheng Li, Yuwei Gu, Shuang Wu and Xinchen Wang
Article Type	Full Research Paper
Supporting Information File 1	Supporting Information.docx; 36.1 KB
ORCID® iDs	Ziheng Li - https://orcid.org/0000-0003-2063-0328

Room-temperature high-performance ammonia gas sensor based on hydroxyapatite film

Mingxu Sun[1], Ziheng Li*[1], Yuwei Gu[1], Shuang Wu[1], Xinchen Wang[1]

Address: [1]Key Laboratory of Physics and Technology for Advanced Batteries (Ministry of Education), College of Physics, Jilin University, No.2699 Qianjin Street, Changchun 130012, China

Email: liziheng@jlu.edu.cn

* Corresponding author

Abstract

A room-temperature high-performance ammonia (NH_3) gas sensor based on hydroxyapatite (HAp) film with three-dimensional network structure was reported in this paper. The gas sensor was fabricated on the indium tin oxide glass (ITO) interdigital electrode via simple electrochemical deposition technique. The HAp film gas sensor shows good sensitivity, high reproducibility and excellent selectivity to NH_3 gas under dry and relative humidity (RH) conditions at room temperature. The response and recovery time of the HAp film gas sensor to 1000 ppm NH_3 gas are 23 s and 14 s under N_2 (dry) condition, and are 4 s and 11 s under air (RH≈30) condition, respectively. The HAp film gas sensor has no considerable deviation in the 1000 ppm NH_3 gas for 3 cycles under N_2 (dry), and so is air (RH≈30) conditions. The HAp film gas sensor shows excellent selectivity to methanol, acetone and ethanol

under N_2 (dry) and air (RH≈30) conditions. Above all, two sensing mechanisms of the HAp film gas sensor to NH_3 gas have been also researched in this work.

Keywords

Hydroxyapatite film; Ammonia gas sensor; Three-dimensional network structure; Sensing mechanisms

Introduction

Ammonia (NH_3), a toxic and corrosive indoor air pollutant, is severe threat to human skin, eye and respiratory tract [1, 2]. Although some traditional methods such as spectroscopic and chromatographic methodologies possess high sensitivity and selectivity, they have limitations of complicated sample preparation and expensive cost [3, 4]. In recent years, a variety of gas sensors based on metal oxides have been extensively investigated [5, 6]. However, they have common problems of poor selectivity, lower response and high operating temperature to gas testing. Another kinds of gas sensors known as conducting polymers have attracted a lot of attention due to their unique electrical properties [7, 8]. But they have the obstacles of low sensitivity, long response time and incomplete desorption of gas molecules to gas testing.

Hydroxyapatite (HAp), a main inorganic component of teeth and bones, has been also investigated in gas testing due to its special functional groups [9, 10]. HAp can be used for NH_3 gas sensing with many advantages, such as high selectivity, short response time and room operating temperature due to its unique sensing mechanisms. However, It still has some challenges need to be broken, such as low response values due to its insufficient surface active sites and practical applications.

Therefore, it is very meaningful to fabricate HAp film gas sensor with excellent sensing performance and practical applications.

The interdigital electrodes having the advantages of reduced impedance, fast establishment of steady-state signals and high signal-to-noise ratio are widely used in sensor research [11, 12]. Electrochemical deposition, is widely used in the preparation of sensing films because it can provide the uniform surface morphology and high conductivity [13]. Combining their advantages, we have proposed a HAp film gas sensor prepared by electrochemical deposition technique based on the ITO interdigital electrode, which have not been reported for gas sensing. Additionally, the three-dimensional network structure with banded crystals of high surface-to-volume ratio was formed in the lift-off space. All these features are important to improve gas sensing performance.

It is well known that reducing the effect of humidity on a gas sensor is important, but the more important thing is to understand the effect of humidity on the sensing mechanisms. This helps improving sensing performance, stability, selectivity and sensitivity. In this work, a novel room-temperature NH_3 gas sensor based on HAp film with three-dimensional network structure was fabricated via a simple electrochemical deposition technique on the ITO interdigital electrode. The HAp film gas sensor shows good sensitivity, high reproducibility and excellent selectivity to NH_3 gas under N_2 (dry) and air (RH≈30) conditions at room temperature. Additionally, two sensing mechanisms of the HAp film gas sensor have been researched. In short, under the N_2 (dry) condition, the —OH acts as adsorption and reaction sites to capture NH_3 molecules on the surface of HAp film. Under the air (RH≈30) condition, the H_2O molecular layers that interacting with the —OH acts as adsorption and reaction sites to capture NH_3 molecules and form hydrogen bonds.

Results and Discussion

Characterization of HAp

Fig. 1 showes XRD patterns of HAp. The characteristic peaks were distinctly observed at 25.9°, 28.1°, 29.0°, 31.7°, 32.2°, 32.9°, 35.8°, 39.2° and 53.6°. The sharp peak at 2θ=25.9°, 32.9°, 35.8°and 53.6° indicates a good crystallization and growth preference on the (0 0 2), (3 0 0), (3 0 1) and (0 0 4) crystal plane. These results confirm the presence of HAp. However, compared with the International Centre for Diffraction Data (ICDD card No. 09-0432), the relative intensities of diffraction peaks are different. The most obvious was that the strongest 2θ peak was the diffraction peak of the (0 0 2) at 25.9° instead of the (2 1 1). This phenomenon is because that the grains grow preferentially perpendicular to the surface of the electrode along the c-axis [14]. Based on this growth mechanism, HAp can provide more OH^- [15], which can provide more adsorption and reaction sites to capture NH_3 molecules on the surface of HAp film, and increase the sensitivity of the gas sensor to NH_3 gas testing.

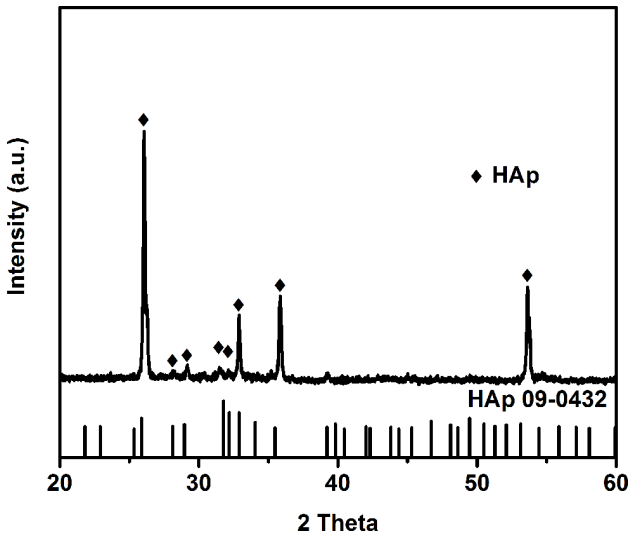

Fig. 1: X-ray diffraction patterns of hydroxyapatite. The bottom is standard patterns (09-0432) for HAp.

Fig. 2 showes the FTIR spectroscopy analysis of HAp. The absorption bands at 3435 and 1634 cm^{-1} corresponded to the water in the air [16]. The visible vibration bands of OH^- were detected at 629 and 3526 cm^{-1}. The vibration bands of PO_4^{3-} were also identified at 1103, 1026, 962, 602 and 561 cm^{-1}, respectively. These results further confirm the presence of HAp.

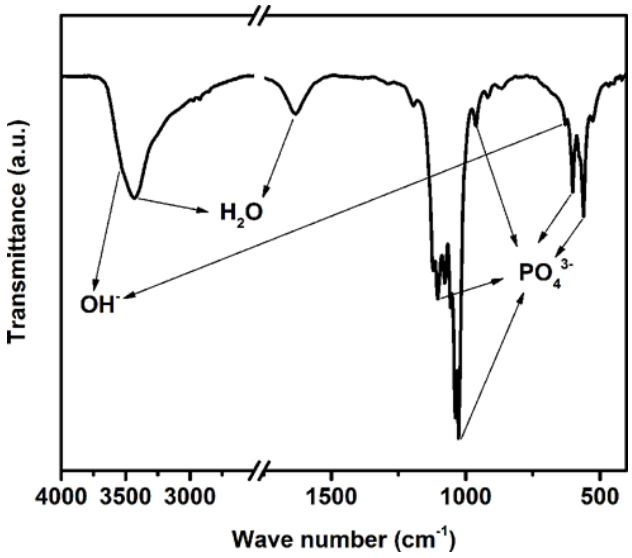

Fig. 2: FTIR spectroscopy analysis of HAp.

Fig. 3 (a) showes the SEM micrographs of ITO interdigital electrode. The middle light-colored segment is glass substrate obtained by photolithography techniques. The dark part of the two sides are ITO glass. The ITO interdigital electrode lift-off space d is about 10 to 25 μm. Fig. 3 (b) showes the SEM micrographs of HAp film gas sensor with uniform surface morphology of coatings. The HAp grows to each other alternately from the two sides of the ITO interdigital electrode, forming a three-dimensional network structure with banded crystals of high surface-to-volume ratio in the lift-off space. Furthermore, most of the HAp grow perpendicularly to the surface of the electrode, which is consistent with the grains growth direction analyzed by XRD. Fig. 3 (c-e) showes the mapping analysis of HAp film gas sensor. All the elements of Ca, P and O can be obviously identified. The EDS analysis (Fig. 3 f) indicated that

the Ca/P molar ration of HAp was 1.72 (>1.67). This probably due to existence Ca^{2+}, which was reacted insufficiently on the HAp film surface. These results further prove the successful preparation of HAp film.

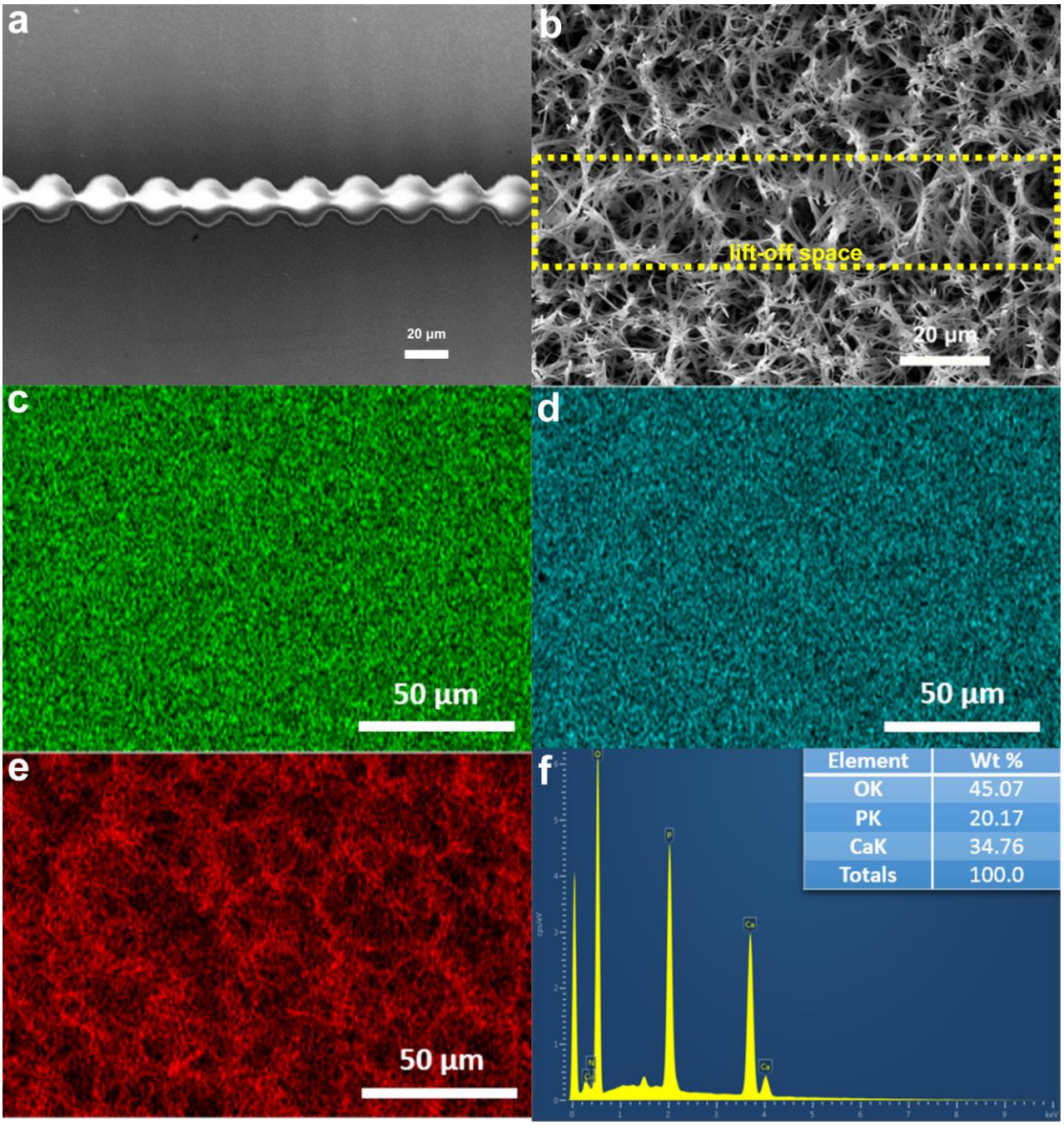

Fig. 3: SEM micrographs of (a) ITO interdigital electrode, (b) HAp film, and element mappings of (c) Ca, (d) P and (e) O, and (f) EDS spectra of the HAp film.

Gas Sensing Properties of HAp Film Gas Sensor

To characterize the sensing performance of the HAp film gas sensor toward NH_3 gas under dry and relative humidity (RH) conditions, the NH_3 gas were tested under N_2 (dry) and air (RH≈30) conditions.

The Fig. 4 (a) shows the sensing performance of the HAp film gas sensor toward 1000 ppm NH_3 gas under N_2 (dry) condition. These data clearly demonstrate fast response region (time=1 s), slow response region (time=22 s) and recovery region (time=14 s). The fast response region is mainly related to physical interactions and the slow response region is mainly related to strong chemical interactions. The Fig. 4 (b) shows the sensing performance of the HAp film gas sensor toward 1000 ppm NH_3 gas under air (RH≈30) condition. These data clearly demonstrate full response region (time=4 s) and recovery region (time=11 s). The NH_3 gas sensing performance were contrast with recently reported works and the results were presented in Table 1. These results indicate that the HAp film gas sensor exhibits outstanding response and recovery time, and good response values. Compared with the N_2 (dry) condition, the HAp film gas sensor under air (RH≈30) condition shows shorter response and recovery time, and stronger saturated response. In other words, the relative humidity condition can help to improve the response values and sensitivity of the HAp film gas sensor toward NH_3 gas. This is because that the HAp film gas sensor is mainly related to strong chemical interactions under N_2 (dry) condition and physical interactions under air (RH≈30) condition to NH_3 gas testing. The sensing mechanisms will be explained in detail in the respective section.

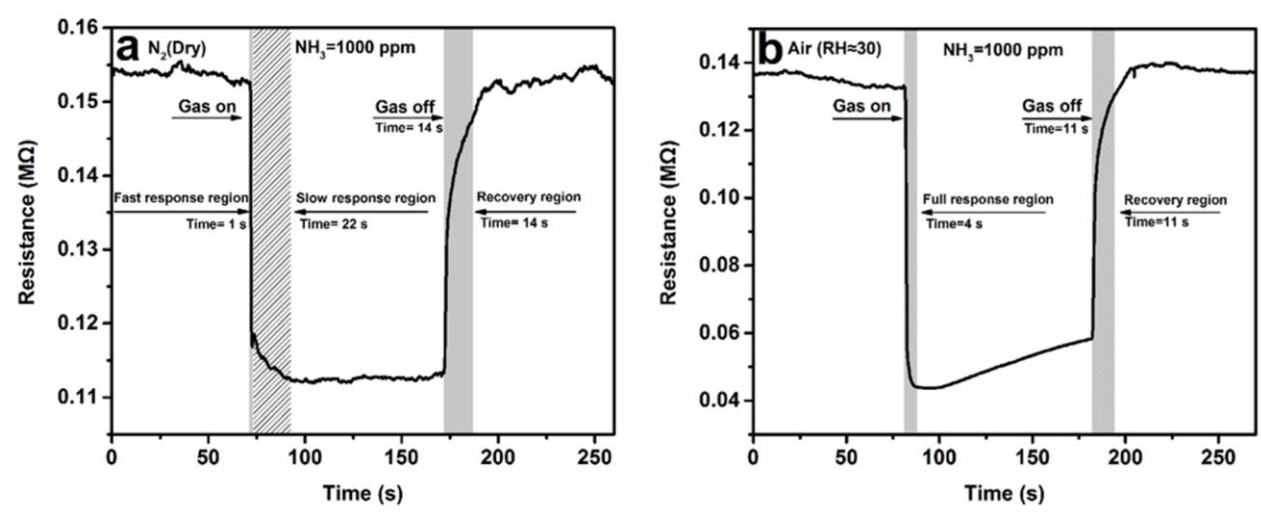

Fig. 4: Sensing performance of the HAp film gas sensor to 1000 ppm NH_3 gas (a) under N_2 (dry) condition, (b) under air (RH≈30) condition.

Table 1: Comparison of NH_3 gas sensing performance of gas sensors reported so far and current work.

Material	Concentration (ppm)	Operating Temperature (℃)	Gas Response	Response Time (s)	Recovery time (s)	Ref.
Mn-ZnO	100	150	28.5	5	15	[18]
Ni-ZnO	100	27	2.52	49	58	[19]
SWCNT	200	RT	3.5	25	20	[20]
rGO	100	RT	65	4	300	[21]
GO-PANI	100	RT	11.3	50	23	[22]
HAp	1000	RT	5.64	23	14	This work
	1000	RT (RH)	13.93	4	11	

Fig. 5 (a) shows the dynamic response curve of the HAp film gas sensor to 100−1000 ppm NH_3 gas under N_2 (dry) condition. It is obviously found that the resistance decreases with the increases of NH_3 gas concentration. The corresponding response values are about 1.08%, 2.73%, 4.38% and 5.64%. The weak response toward N_2 is mainly related to porous structure of HAp surface. The characterization of the HAp film pore size distribution is shows in Fig. S1, conforming porous structure of the HAp film. Fig. 5 (b) shows the dynamic response curve of the HAp film gas sensor to 100−1000 ppm NH_3 gas under air (RH≈30) condition. It is obviously found that the resistance decreases with the increases of NH_3 gas concentration. The corresponding response values are about 2.82%, 5.41%, 9.00% and 13.93%. The response toward air is mainly related to physical interactions between H_2O molecules and HAp surface. The response values of the HAp film gas sensor to 100 ppm NH_3 gas under air (RH≈30) condition was 2.69 times higher than that under N_2 (dry) condition.

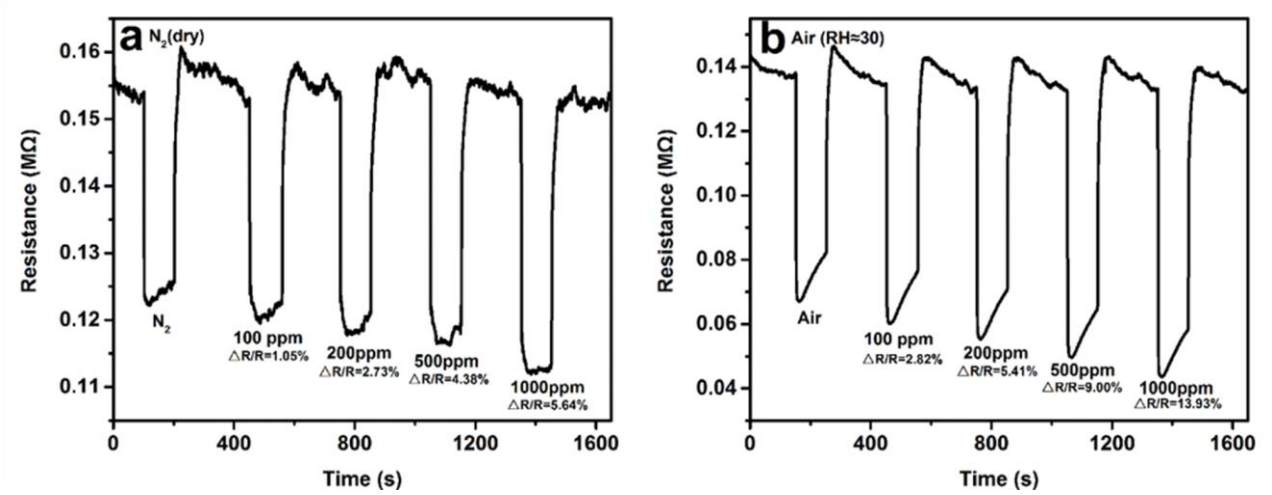

Fig. 5: Dynamic response curve of the HAp film gas sensor to 100−1000 ppm NH_3 gas (a) under N_2 (dry) condition, (b) under air (RH≈30) condition.

The reproducibility of the HAp film gas sensor is further tested toward 1000 ppm NH_3 gas for 3 cycles under N_2 (dry) and air (RH≈30) conditions in Fig. 6 (a-b). It has no considerable deviation in the NH_3 gas response (<5%) with excellent recovery under all conditions.

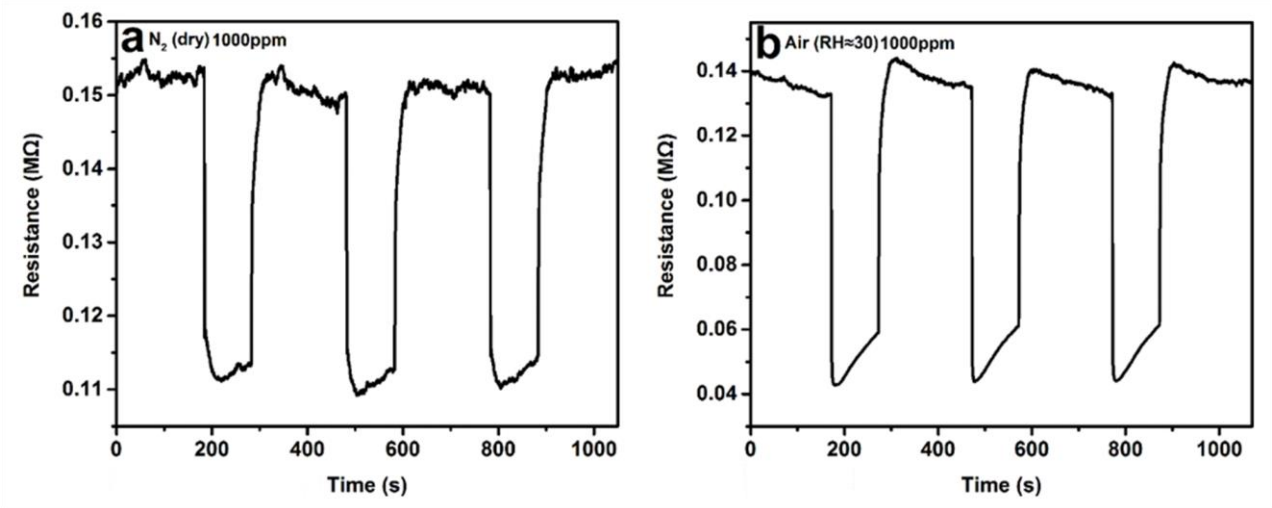

Fig. 6: Reproducibility of the HAp film gas sensor to 1000 ppm NH_3 gas for 3 cycles (a) under N_2 (dry) condition, (b) under air (RH≈30) condition.

Gas Selectivity of HAp Film Gas Sensor

Fig. 7 shows the response values of the HAp film gas sensor towards 1000 ppm ammonia, methanol, acetone and ethanol under N_2 (dry) and air (RH≈30) conditions, respectively. Although the HAp film gas sensor shows slight response under N_2 (dry) condition, the response under air

(RH≈30) condition is negligible to 1000 ppm methanol, acetone and ethanol. This phenomenon can be explained by the special sensing mechanisms of HAp film gas sensor to NH_3 gas. Under the N_2 (dry) condition, the —OH acts as adsorption and reaction sites to capture gas molecules on the surface of HAp film. Therefore, all of the above gases have slight response. The difference is that the interaction between ammonia and —OH is stronger than the other three kinds of gases. Under the air (RH≈30) condition, the H_2O molecular layers that interacts with the —OH acts as adsorption and reaction sites to capture the NH_3 molecules and form hydrogen bonds. The difference is that the other three kinds of gases are difficult to utilize the adsorption and reaction sites formed by the H_2O molecular layers, and the H_2O molecular layers will occupy the original —OH adsorption and reaction sites to capture the gas molecules. Therefore, other three kinds of gases response is very low. The selectivity test indicates that the NH_3 gas sensor is reliable and promising for practical use.

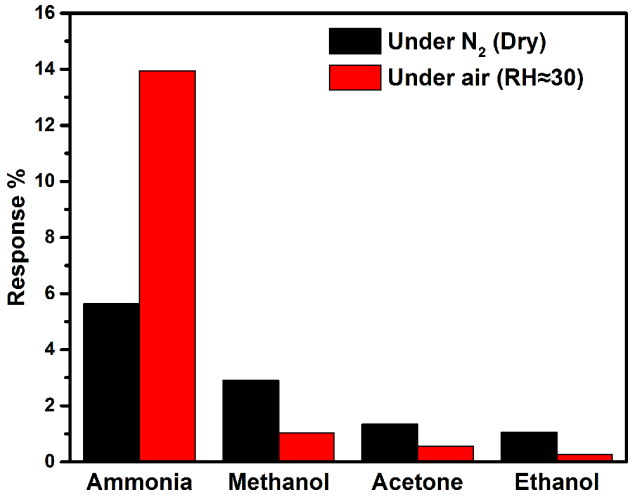

Fig. 7: Response values of the HAp film gas sensor to 1000 ppm ammonia, methanol, acetone and ethanol under N_2 (dry) and air (RH≈30) conditions.

Gas Sensing Mechanisms of HAp film

Under the N_2 (dry) condition (Fig. 8 (a)), the HAp film gas sensor is mainly related to strong chemical interactions to NH_3 gas testing. The —OH acts as adsorption and reaction sites to capture NH_3 molecules on the surface of HAp film. NH_3 molecules can enhance the conductivity of HAp film gas sensor, so the resistance decreases. Under the air (RH≈30) condition (Fig. 8 (b)), the HAp film gas sensor is mainly related to physical interactions to NH_3 gas testing. The H_2O

molecular layers was firstly physiosorbed by—OH on the surface of HAp film. More H_2O molecules were physiosorbed through single hydrogen bonding, and multi H_2O molecular layers were formed [17]. The H_2O molecular layers that interacts with the —OH acts as adsorption and reaction sites to capture NH_3 molecules and form hydrogen bonds. NH_3 molecules can interact with H_2O molecules and dissociate to NH_4^+ and OH^- on the surface of HAp film ($NH_3 + H_2O \rightarrow NH_3{\cdot}H_2O \rightarrow NH_4^+ + OH^-$). NH_4^+ can transfer along the electrode surface, so the resistance decreases. More importantly, the air condition can provide more adsorption and reaction sites through single hydrogen bonding of multi H_2O molecular layers. In other words, H_2O molecules can improve sensitivity for NH_3 gas testing.

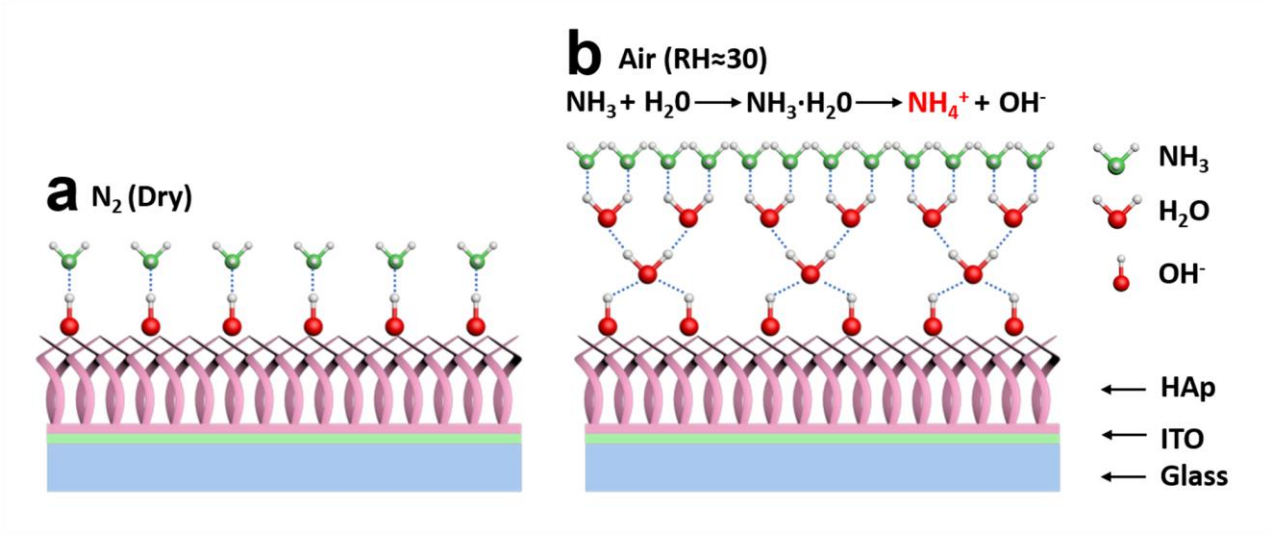

Fig. 8: Schematic illustration for sensing mechanisms of the HAp film sensor (a) under N_2 (dry) condition, (b) under air (RH≈30) condition.

Conclusion

In conclusion, a novel room-temperature NH_3 gas sensor based on banded crystals HAp film was developed on the ITO interdigital electrode by electrochemical deposition technique. Because of the —OH on the surface, high conductivity and three-dimensional network structure with the high surface-to-volume ratio, the HAp film gas sensor exhibits good sensitivity, high reproducibility and excellent selectivity to NH_3 gas under N_2 (dry) and air (RH≈30) conditions at room temperature.

Moreover, two sensing mechanisms of the HAp film gas sensor were proposed. In brief, under the N_2 (dry) condition, the —OH acts as adsorption and reaction sites to capture NH_3 molecules on the surface of HAp film. Under the air (RH≈30) condition, the H_2O molecular layers that interacts with the —OH acts as adsorption and reaction sites to capture NH_3 molecules and form hydrogen bonds.

Experimental

Materials

Calcium nitrate ($Ca(NO_3)_2 \cdot 4H_2O$) and ammonium secondary phosphate ($(NH_4)_2HPO_4$) were purchased from Tianjin Guangfu Fine Chemical Research Institute. Phosphoric acid (H_3PO_4) were obtained from Beijing Chemical Works. All reagents were of analytical reagent grade and all solutions were prepared using deionised water.

Characterization

The X-ray diffraction (XRD) patterns of the specimens were conducted on a Rigaku MiniFlex 600 X-ray diffractometer with an angular range of 20°~60°. The Fourier transform infrared spectroscopy were measured by VERTEX 70 FT-IR Spectrometer (BRUKER, Germany). Scanning electron microscopic (SEM) images were taken on FEI Magellan 400 (FEI Corp., Netherlands). Gas sensor tests were performed with a CS 300H electrochemical workstation (Wuhan Corrtest Instruments Corp., China) in a two-electrode set up and stainless steel chamber (Zhengzhou Ketan Instrument and Equipment Corp., China). The pore size distributions were measured by the Barrett-Joyner-Halenda (BJH) method.

Gas Sensor Fabrication

The ITO glass substrate (8 × 50 mm) was cleaned by ethanol to remove the contamination. The patterns of ITO interdigital electrode was achieved by the conventional photolithography techniques. There are two sides of ITO interdigital electrode, electrode A and electrode B, they are no-conductive to each other. The ITO interdigital electrode lift-off space d is about 10 to 25 μm. The illustration of ITO interdigital electrode is showed in Scheme 1.

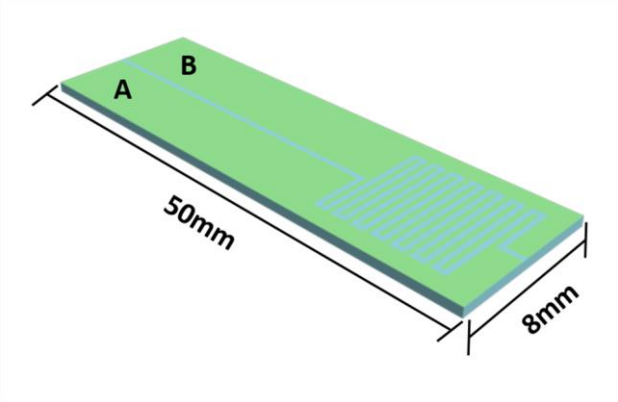

Scheme 1: Schematic illustration of ITO interdigital electrode.

The ITO interdigital electrode used for modification was treated by ultrasonic in the acetone/ethanol mixture solution (volume ratio was 1:1) for 20 min and was cleaned by deionized water. The electrolyte was prepared by mixing the solution containing $Ca(NO_3)_2$ of 0.20 mol/L, $(NH_4)_2HPO_4$ of 0.067 mol/L and H_3PO_4 of 0.053 mol/L. The pH of electrolyte was 6.2. The electrochemical deposition was performed in a beaker using a two electrodes configuration. The ITO interdigital electrode formed by the parallel connection of electrode A and electrode B was served as cathode and platinum electrode was served as anode. The electrochemical deposition was carried out in potentiostatic mode by applying a potential of 2.35 V at 60℃ during 120 min through a DC power supply MT 152D (MAISHENG, China). The HAp film electrode was obtained by washing with deionized water and dried in a drying oven at 60 °C for

10 minute. Eventually, the electrode was cutting into standards of 8×20 mm for the NH_3 gas sensor.

Gas sensor Test

The schematic illustration of the experimental setup used for gas sensor property test is depicted in Scheme 2. The gas sensor was fixed inside the vacuum test chamber. The resistance of the gas sensor was measured at constant potential (1 V) through electrochemical workstation, and working electrode and auxiliary electrode of electrochemical workstation are connected to electrode A and electrode B respectively in the chamber. The chamber has the facility of inlet and outlet of the gas. Before the test, the chamber was evacuated by the vacuum pump and the pressure inside the gas chamber was measured by the vacuum gauge attached to the chamber. Different concentrations of NH_3 gas ranging from 100 to 1000 ppm were prepared with gas sampling bags, which connected to the chamber for the measurements on NH_3 gas at room temperature. The HAp film gas sensor properties were tested by measuring the change in the initial resistance of the gas sensor upon controlled exposure to NH_3 gas. The percentage change of the gas response S (%) is defined using the following equations:

$$\Delta R = R_g' - R_g \quad (1)$$

$$S(\%) = \frac{\Delta R}{R} \times 100 \quad (2)$$

where R are the sensor resistance in vacuum condition, R_g' are the sensor resistance in N_2 or air, and R_g are the sensor resistance in testing gas under N_2 or air conditions.

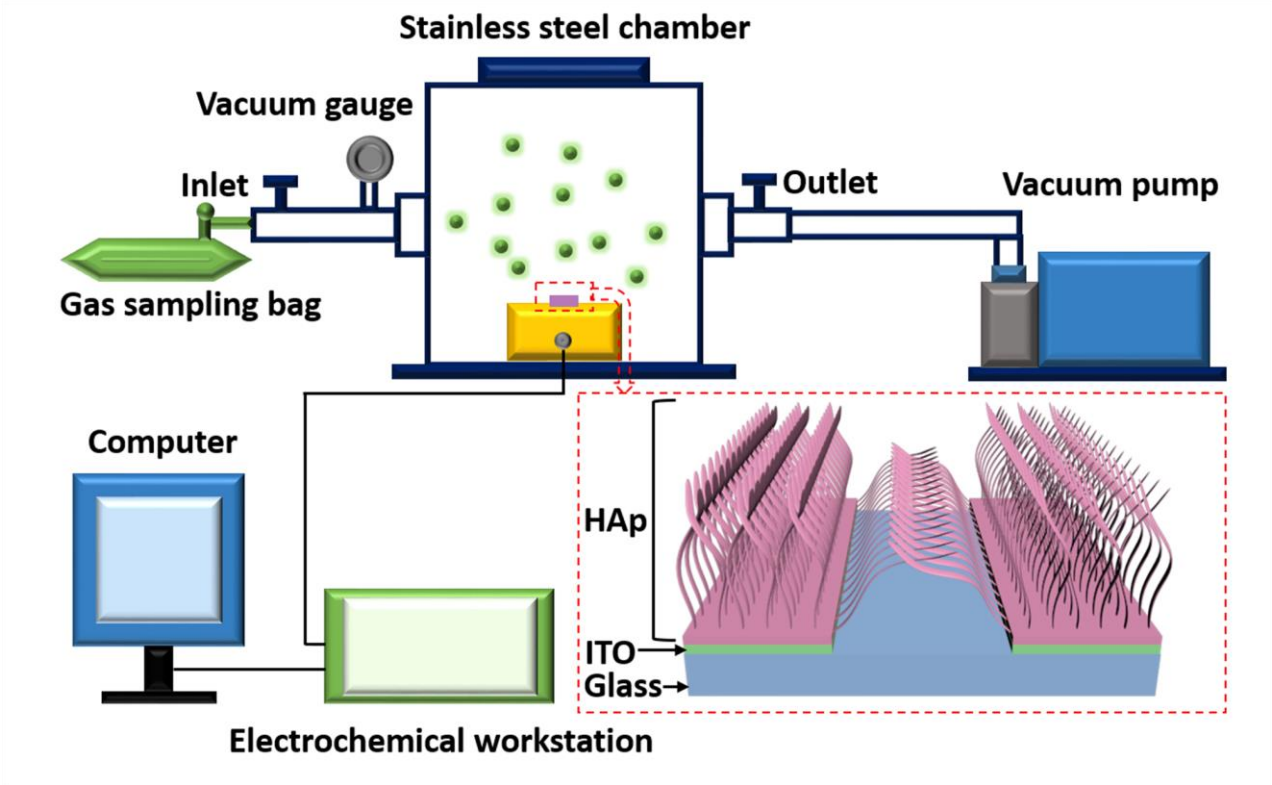

Scheme 2: Schematic illustration of the experimental setup used for gas sensor property test.

Supporting Information

The characterization of the HAp film pore size distribution is showed in Fig. S1, conforming porous structure of the HAp film.

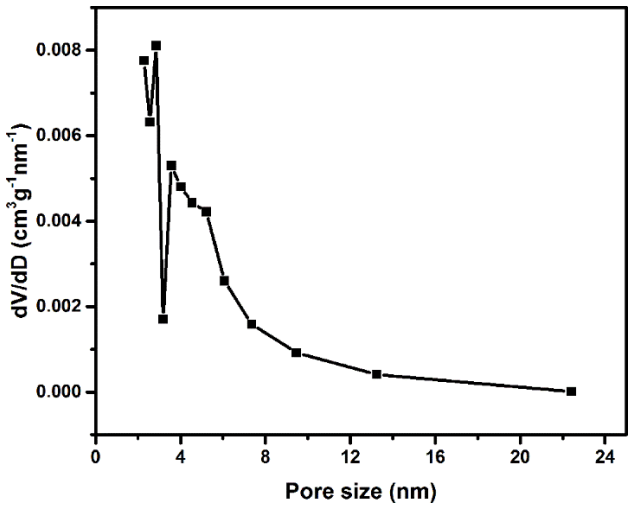

Fig. S1: Pore size distribution of HAp film, calculated by the BJH method.

Acknowledgements

This work was supported by the national long-term project (No.WQ20142200205) of “Thousand Talents Plan of Foreign Experts Affairs” of People Republic of China.

References

1. C. Lousteau, M. Besson, C. Descorme, *Catalysis Today* **2015**, *241*, 80-85 doi: 10.1016/j.cattod.2014.03.043.

2. D. Zhang, J. Liu, C. Jiang, A. Liu, B. Xia, *Sensors and Actuators B-Chemical* **2017**, *240*, 55-65 doi: 10.1016/j.snb.2016.08.085.

3. X. D. Wang, O. S. Wolfbeis, *Anal Chem* **2013**, *85*, 487-508 doi: 10.1021/ac303159b.

4. B. Timmer, W. Olthuis, A. v. d. Berg, *Sensors and Actuators B: Chemical* **2005**, *107*, 666-677 doi: 10.1016/j.snb.2004.11.054.

5. K. Shingange, Z. P. Tshabalala, O. M. Ntwaeaborwa, D. E. Motaung, G. H. Mhlongo, *J Colloid Interface Sci* **2016**, *479*, 127-138 doi: 10.1016/j.jcis.2016.06.046.

6. C. Wang, X. Li, F. Xia, H. Zhang, J. Xiao, *Sensors and Actuators B: Chemical* **2016**, *223*, 658-663 doi: 10.1016/j.snb.2015.09.145.

7. A. L. Sharma, K. Kumar, A. Deep, *Sensors and Actuators A: Physical* **2013**, *198*, 107-112 doi: 10.1016/j.sna.2013.04.026.

8. S. Carquigny, J. B. Sanchez, F. Berger, B. Lakard, F. Lallemand, *Talanta* **2009**, *78*, 199-206 doi: 10.1016/j.talanta.2008.10.056.

9. L. Huixia, L. Yong, T. Yanni, L. Lanlan, Z. Qing, L. Kun, T. Hanchun, *New Journal of Chemistry* **2015**, *39*, 3865-3874 doi: 10.1039/c4nj02352h.

10. Y. Tan, H. Li, Y. Liu, J. Xie, J. He, J. Pan, *RSC Advances* **2016**, *6*, 76874-76878 doi: 10.1039/c6ra12334a.

11. A. V. Mamishev, K. Sundara-Rajan, F. Yang, Y. Q. Du, M. Zahn, *Proceedings of the Ieee* **2004**, *92*, 808-845 doi: 10.1109/jproc.2004.826603.

12. R. Igreja, C. J. Dias, *Sensors and Actuators A: Physical* **2004**, *112*, 291-301 doi: 10.1016/j.sna.2004.01.040.

13. M. Sun, Z. Li, S. Wu, Y. Gu, Y. Li, *Electrochimica Acta* **2018**, *283*, 1223-1230 doi: 10.1016/j.electacta.2018.07.019.

14. M. H. Cao, Y. H. Wang, C. X. Guo, Y. J. Qi, C. W. Hu, *Langmuir* **2004**, *20*, 4784-4786 doi: 10.1021/la0498197.

15. N. H. de Leeuw, *Phys. Chem. Chem. Phys.* **2004**, *6*, 1860-1866 doi: 10.1039/b313242k.

16. H. Ye, X. Y. Liu, H. Hong, *J Mater Sci Mater Med* **2009**, *20*, 843-50 doi: 10.1007/s10856-008-3647-3.

17. S. W. Chen, O. K. Khor, M. W. Liao, C. K. Chung, *Sensors and Actuators B: Chemical* **2014**, *199*, 384-388 doi: 10.1016/j.snb.2014.03.057.

18. R. S. Ganesh, E. Durgadevi, M. Navaneethan, V. L. Patil, S. Ponnusamy, C. Muthamizhchelvan, S. Kawasaki, P. S. Patil, Y. Hayakawa, *Journal of Alloys and Compounds* **2017**, *721*, 182-190 doi: 10.1016/jjallcom.2017.05.315.

19. G. K. Mani, J. B. B. Rayappan, *Applied Surface Science* **2014**, *311*, 405-412 doi: 10.1016/j.apsusc.2014.05.075.

20. M. Y. Lone, A. Kumar, S. Husain, M. Zulfequar, Harsh, M. Husain, *Physica E: Low-dimensional Systems and Nanostructures* **2017**, *87*, 261-265 doi: 10.1016/j.physe.2016.10.049.

21. Q. Feng, X. Li, J. Wang, A. M. Gaskov, *Sensors and Actuators B-Chemical* **2016**, *222*, 864-870 doi: 10.1016/j.snb.2015.09.021.

22. Z. Wu, X. Chen, S. Zhu, Z. Zhou, Y. Yao, W. Quan, B. Liu, *Sensors and Actuators B: Chemical* **2013**, *178*, 485-493 doi: 10.1016/j.snb.2013.01.014.